

Perturbation analysis of steady and unsteady electrohydrodynamic chaotic advection inside translating drops

Fan Wu,^{1,2} Dmitri Vainchtein,^{1,3} and Thomas Ward⁴

¹*Department of Mechanical Engineering, Temple University, Philadelphia, Pennsylvania 19122, USA*

²*School of Traffic and Transportation Engineering, Central South University, Changsha 410075, China*

³*Space Research Institute, Moscow, GSP-7, 117997, Russia*

⁴*Department of Aerospace Engineering, Iowa State University, Ames, Iowa 50011-2271, USA*

(Received 11 May 2015; published 27 August 2015; corrected 17 March 2016)

A drop translating in the presence of an electric field is studied analytically. The flow is a combination of a Hadamard-Rybczynski and a Taylor circulation due to the translation and electric field, respectively. We consider chaotic advection that is generated by (1) tilting and (2) time-dependent modulation of the electric field. For the analysis we consider small perturbations in time and space to what is otherwise an integrable flow. By using a robust analytical technique we find an adiabatic invariant (AI) for the system by averaging the equations of motion. The chaotic advection is due to quasirandom jumps of the AI after crossing the separatrix of the unperturbed flow. We demonstrate that the asymptotic analysis leads to a set of criteria that can be used to optimize stirring in these systems.

DOI: [10.1103/PhysRevE.92.023030](https://doi.org/10.1103/PhysRevE.92.023030)

PACS number(s): 47.52.+j, 05.45.Pq, 47.15.G–, 47.51.+a

I. INTRODUCTION

Transport of scalar quantities such as heat and/or mass from translating drops is typically controlled by diffusion. This is due to the fact that the steady axisymmetric streamlines are closed, with the consequence that transport remains diffusion limited at high Pe [1]. It has been proposed that stirring inside of the dispersed phase by chaotic advection may lead to enhanced transport. The belief is that complex-internal circulations inside of a translating drop [2–9] or even a stationary bounded domain [10,11] will lead to a breakup of the closed streamlines associated with an axisymmetric flow. Subsequently a fluid particle trajectory occupies a larger domain and therefore mass transport is not necessarily diffusion limited [12]. There is one main caveat to this theory since sampling a larger domain does not imply sampling the total domain. So even a chaotic flow field can experience ordered domains called Kolmogorov-Arnold-Moser (KAM) regions where mass transport can still be diffusion limited. Determining the conditions for the appearance of these regions is necessary to produce a robust qualitative approach to enhanced interphase transport. But it can be elusive since it requires accurate computation of differential equations that contain intrinsic stiffness due to the complexity of the flows.

Chaotic flow fields have been generated by taking advantage of the linearity associated with incompressible low-Reynolds-number circulations inside of drops or Stokes flow conditions. Under these conditions it is possible to use the superposition principle to add any number of flows to a base or stationary flow $\mathbf{v}(\mathbf{x},t) = \sum \mathbf{v}_i(\mathbf{x},t)$. These flows are characterized as linear (shear flow), quadratic (translation, Hill's spherical vortex, Hadamard-Rybczynski), cubic (quadrupole, Taylor circulation), and higher order. Then, by carefully solving the advection equation

$$\dot{\mathbf{x}} = \mathbf{v}(\mathbf{x},t), \quad (1)$$

it is possible to determine individual particle trajectories. Here and throughout the overdot denotes a derivative with respect to time. The two main techniques for determining the

presence of deterministic chaos in superimposed flow fields has been through Poincaré mapping and calculating Lyapunov exponents. Each has advantages and disadvantages where Poincaré mapping of individual (long-time analysis) or many (short-time analysis) fluid particles is extremely accurate in mapping ordered regions. It is computationally costly, though, and requires highly accurate implicit numerical solvers since stiff equations must be advanced in time, possibly over long periods. Lyapunov exponents provide information for the rate of divergence of trajectories initially in close proximity. But these exponents are only valid over short times and can provide nonphysical results where the rate of divergence (based on a linearization of the velocity field) can produce fluid particle displacements that exceed the boundaries of the domain.

The field of chaotic advection inside drops has been divided into two main types of flow: axisymmetric unsteady and three-dimensional (3D) steady. Although axisymmetric unsteady flows are analytically and computationally less intensive than their three-dimensional steady flow counterparts, the first systems to be studied were of the three-dimensional flavor. Bajer and Moffatt [10], were the first to analyze and compute steady three-dimensional flows inside drops. They treated general bounded quadratic flows in the context of fast dynamo action caused by the Earth's magnetic field. These authors showed that such flows could exhibit “stretch-twist-fold” (STF) kinematics and that these were the necessary ingredients that lead to chaotic advection. Stone, Nadim, and Strogatz [2] and Stone and Kroujiline [13] analyzed numerically the possibility of chaotic advection in a steady three-dimensional Stokes flow. Stone and Kroujiline [13] considered two possible three-dimensional internal velocity fields. The first consisted of a drop translating due to buoyancy forces and the second a drop in an extensional flow. The addition of a vorticity vector that is not aligned to the axis of each of these velocity fields produced steady three-dimensional chaotic streamlines. A computational parametric study of the mixing was performed through an analysis of Poincaré maps.

More recently, unsteady axisymmetric flows have been developed to address the need to validate many of the underlying chaotic advection concepts through experimentation. This is a natural consequence of the fact that axisymmetric flows are generally easier to study experimentally when considering the advancement of laser techniques to analyze flow fields [14]. Furthermore, it has been shown that it is possible to produce one-to-one comparisons between experimental and computationally generated short-time Poincaré maps in axisymmetric flows [6]. The types of axisymmetric flows, though, that can be generated experimentally are limited to a superpositioning of the quadratic translation flow and quadrupole generated by electrohydrodynamics [4–6]. Nevertheless, more precise details have been provided by studying the axisymmetric systems, where it is now generally understood that efficient stirring inside of a drop requires the presence of an internal hyperbolic fixed point. For the case of the axisymmetric flow this produces a stagnation plane that separates the counter-rotating toroidal elliptic points caused by the quadrupole circulation. Then by modulating the location of the stagnation plane, where some trajectories must cross, it is possible to generate a domain where efficient stirring occurs i.e., fluid particle trajectories sample a larger fluid domain than without modulation of the stagnation plane.

This concept of crossing a stagnation plane, or a separatrix, to generate efficient stirring has a fairly robust history in the context of dynamical systems. Neishtadt [15] and Cary *et al.* [16] were apparently the first to study small perturbations of a particle's trajectory as a means to efficient stirring of a fixed domain. The Neishtadt analysis has been applied to steady three-dimensional systems where, in two separate studies [3,17], an averaging-perturbation analysis method was applied to the flow situations proposed by Bajer and Moffatt [10] and by Stone and Kroujiline [13]. In the former case the unperturbed flow is the axisymmetric quadrupole circulation and the perturbation is the addition of a rotation in the drop with a slight tilt. The change that a Lagrangian particle undergoes predicted from the analysis was in good agreement with numerical simulation of the full three-dimensional equations of motion. The results show that even small tilt $O(\epsilon)$, ($\epsilon \ll 1$) can produce $O(1)$ regions of mixing due to multiple separatrix crossings of individual fluid particles.

Neishtadt's averaging method involves treating one flow as a base flow and linearizing the other in terms of a perturbative expansion. The motions are separated into fast and slow, where the fast motion typically involves the motion around an elliptic point of the unperturbed system, $s = f(\dot{r}, \dot{\theta})$. The two slow motions are (1) perturbations from a two-dimensional to a three-dimensional flow which typically involve motions in the azimuthal direction, ϕ , and (2) the change in mass transport across streamlines from the stream function ψ of the unperturbed flow. By averaging the slow motions over the fast, the three-dimensional system is approximately two dimensional with some perturbation. Then, by focusing on a region in the vicinity of the separatrix of the unperturbed flow (SUF), it is possible to characterize changes to an adiabatic variant (AI) Φ in terms of the slow motions. Motion along the AI that do not cross the separatrix are clearly KAM regions since their Φ value is constant in the slow variable domain.

Here we propose a perturbative analysis of two cases: (1) a drop translating in the presence of an electric field that is not parallel to the direction of displacement and (2) an axisymmetric unsteady flow caused by a drop translating in the presence of a modulated electric field. In the next section details describing the electrohydrodynamically generated flow are discussed along with a description of the unperturbed system. Then the three-dimensional problem is presented using the perturbation expansion proposed by Neishtadt. A novel approach to the axisymmetric unsteady problem is presented in the following section. Finally, a discussion of both analyses is presented along with some future direction for the analytical methods followed by concluding remarks.

II. PROBLEM STATEMENT: ELECTROHYDRODYNAMICALLY DRIVEN STIRRING INSIDE A DROP

Consider a drop of radius a translating in the presence of a spatially uniform steady electric field denoted \mathbf{E} . The drop is assumed to remain spherical such that drop deformation due to the electric stresses and viscous stresses, or, equivalently, the capillary numbers Ca_E and Ca_U , respectively, are assumed small ($\ll 1$). The physical parameters are the resistivities $1/\sigma_i$, the electric permittivities $\kappa_0\kappa_i$ (where κ_0 is the electric permittivity constant), the absolute viscosities μ_i , and the densities ρ_i , where subscripts 1,2 will denote the continuous and dispersed phases, respectively. The incompressible flow depends on the dimensionless property ratios $X = \sigma_2/\sigma_1$, $S = \kappa_1/\kappa_2$, and $\lambda = \mu_2/\mu_1$. Under Stokes flow condition the drop settles with characteristic velocity U . The characteristic velocity generated by the electric field V is proportional to $|E|^2$ [18,19]. Then the dimensionless velocity written as $W = 4V(1 + \lambda)/U$ represents the relative strength of the Taylor to the Hadamard-Rybczynski circulations.

Now we ask the following question: How can we modify the base flow to stir the fluid inside the drop, preferably in a domain the size of which can also be controlled. There are two natural ways to achieve this. First, we can tilt the electric field, thus breaking the axial symmetry (this method is discussed in the next section). Alternatively, we can make the amplitude of the field oscillate in time, thus breaking the autonomy of the flow (Sec. IV). It is the objective of the paper to compare those two approaches. Note that as the approaches are somewhat similar, the derivations have a lot in common. Therefore, we put most of the explanations in the next section, and this is followed by the analysis using these two approaches.

A. Unperturbed velocity field

The base flow is a superposition of the aligned version of the steady Taylor and steady Hadamard-Rybczynski circulations. In this case the flow is axisymmetric and is defined by a stream function $\psi = \psi_B + W\psi_E$:

$$\psi = (r^4 - r^2) \sin^2 \theta + W(r^3 - r^5) \sin^2 \theta \cos \theta, \quad (2)$$

where ψ_B is the stream function for the Hadamard-Rybczynski circulation and ψ_E for the Taylor circulation. The stream function is related to a two-dimensional velocity according to the expression $\mathbf{v} = \nabla \times \boldsymbol{\psi}$ where the vector potential for

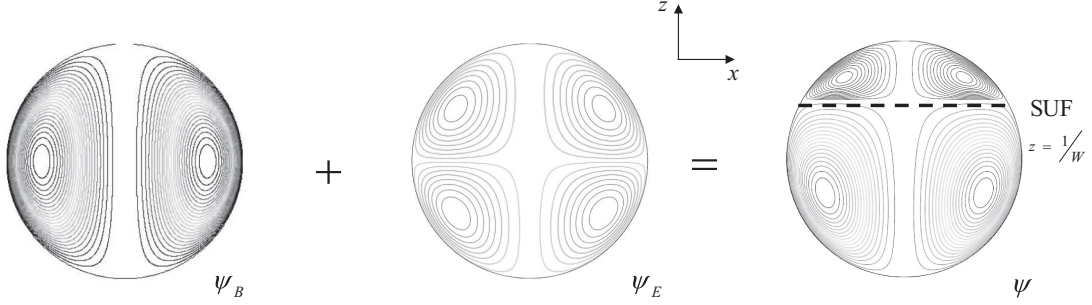


FIG. 1. Assembly of Hadamard-Rybczynski and Taylor circulations yields the unperturbed flow structure.

the stream function is defined $\psi = (0, 0, \psi/r \sin \theta)$ in spherical coordinates. The quadrupole structure of the Taylor circulation is characterized by stagnation points at the equator and the poles along the interface. The four stagnation points are joined by a hyperbolic fixed point at the drops center. The spherical vortex structure of the Hadamard-Rybczynski circulation is characterized by two stagnation points at the poles. For large-enough values of W the quadrupole structure of the Taylor circulation is preserved with some offset in the stagnation points at the center and the equator due to the Hadamard-Rybczynski circulation. The segment joining the stagnation point on the vertical axis with the points on the surface of the sphere is the separatrix of interest. The separatrix lies on a horizontal plane, the axial location from the center of the drop given by $1/W$ [20].

The function ψ plays the role of a stream function: At any fixed moment of time the velocity field (3) satisfies

$$\dot{r} = \frac{1}{r^2 \sin \theta} \frac{\partial \psi}{\partial \theta}, \quad \dot{\theta} = -\frac{1}{r \sin \theta} \frac{\partial \psi}{\partial r}.$$

Note that ψ is a classical axisymmetric stream function in a sense that streamlines are the line of constant ψ for a fixed value of ϕ .

It follows from (2) that the advection equations (or equations of motion) are

$$\begin{aligned} \dot{r} &= 2(r^2 - 1) \cos \theta + W(r - r^3)(3 \cos \theta - 1) \\ \dot{\theta} &= \frac{2}{r}(1 - 2r^2) \sin \theta + W(5r^2 - 3) \sin \theta \cos \theta \\ \dot{\phi} &= 0. \end{aligned} \quad (3)$$

Clearly, flow (3) possesses two integrals: the azimuthal angle ϕ and the stream function ψ . Therefore, all the streamlines, except for those passing through the singular points discussed above, are closed curves. A typical phase portrait is shown in Fig. 1.

III. STEADY THREE-DIMENSIONAL FLOW

The first application of the averaging technique for electrohydrodynamically driven stirring involves a classic example of a bounded three-dimensional flow. To generate a three-dimensional flow a steady electric field is tilted by an angle α relative to the drops settling motion as shown in Fig. 2. In Cartesian coordinates the velocity field for this flow is written

as $\mathbf{v}(\mathbf{x}, \mathbf{x}_\alpha) = \mathbf{v}_H(\mathbf{x}) + \mathbf{J}(\alpha)\mathbf{v}_E(\mathbf{x}_\alpha)$, where

$$\mathbf{J}(\alpha) = \begin{pmatrix} \cos \alpha & 0 & \sin \alpha \\ 0 & 1 & 0 \\ -\sin \alpha & 0 & \cos \alpha \end{pmatrix}$$

is a Jacobian matrix, and

$$\begin{aligned} x_\alpha &= x \cos \alpha - z \sin \alpha \\ z_\alpha &= z \cos \alpha + x \sin \alpha. \end{aligned}$$

Under these conditions the flow inside the drop is chaotic where streamlines fill a large portion of either the northern or southern hemisphere, or both, depending on the initial conditions. The flow is unique for an internal circulation since it possesses a plane of symmetry located at $y = 0$ for $0 < \alpha < \pi/2$. When the electric field orientation is perpendicular to the translational motion, $\alpha = \pi/2$, then another symmetry plane forms, dividing the drop into four cells when viewed along the translational axis. The presence of the symmetry plane was experimentally verified in Ref. [9].

We are interested in the situation when the tilt angle α of the Taylor circulation relative to the Hadamard-Rybczynski circulation is small or $\cos \alpha \approx 1$ and $\sin \alpha \approx \epsilon$ for $\epsilon \ll 1$ and the coordinates of the Taylor circulation \mathbf{x}_α [9] are $x_\epsilon = x - \epsilon z$ and $z_\epsilon = z + \epsilon x$. The resulting velocity field $\mathbf{v} = \mathbf{v}_{H+E} + \epsilon \mathbf{v}_\epsilon$ in spherical coordinates is

$$\begin{aligned} \dot{r} &= 2(r^2 - 1) \cos \theta + W(r - r^3)(3 \cos \theta - 1) \\ &\quad + \epsilon W 6r \cos \phi \sin \theta (1 - r^2) \\ \dot{\theta} &= \frac{1}{r}(2 - 4r^2) \sin \theta + W(5r^2 - 3) \sin \theta \cos \theta \\ &\quad + \epsilon W(5r^2 - 3) \cos \phi (1 - 2 \cos^2 \theta) \\ \dot{\phi} &= \epsilon W(5r^2 - 3) \sin \phi \cot \theta, \end{aligned} \quad (4)$$

where $\mathbf{v}_{H+E} = \mathbf{v}_H + \mathbf{v}_E$ is the sum of the unperturbed-axisymmetric velocity fields.

A. Averaging method and phase portraits of the averaged system

We now apply the averaging technique developed by Neishtadt *et al.* [3, 17] to flow (4). By averaging we develop a mathematical expression for the adiabatic invariant Φ for the perturbed system. A point inside the drop that does not lie on the z axis can be specified by the coordinates ψ , ϕ , and s , where ψ and ϕ are the values of the unperturbed system integrals and $s(\text{mod } 2\pi)$ is the phase (angle variable) along the unperturbed

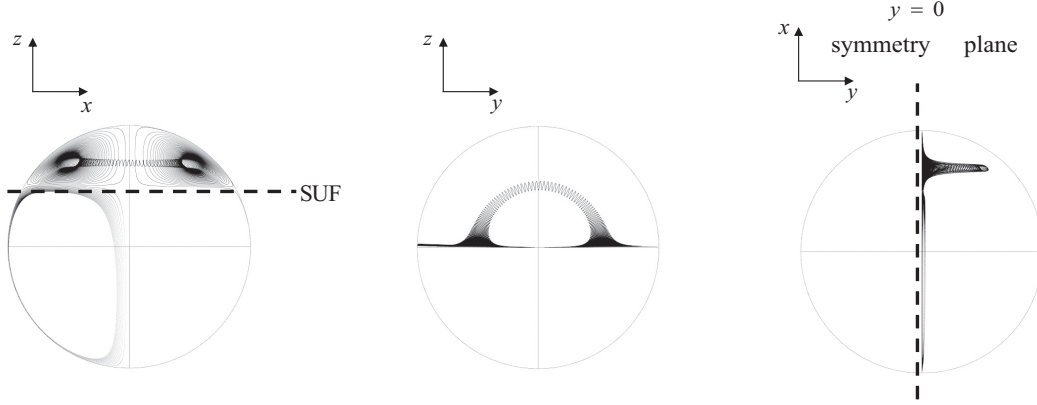


FIG. 2. Assembly of Hadamard-Rybczynski and Taylor circulations yields a perturbed steady flow structure for $\epsilon = 0.01$. The three-dimensional trajectory is viewed using the xz , yz , and xy planes, respectively.

streamline passing through the point under consideration. In terms of new variables the equation of motions can be written as:

$$\begin{aligned} \dot{\psi} &= \epsilon f(\psi, \phi, s), & \dot{\phi} &= \epsilon g(\psi, \phi, s), \\ \dot{s} &= \Omega(\psi) + \epsilon h(\psi, \phi, s), \end{aligned} \quad (5)$$

where $\Omega(\psi)$ is the frequency around a closed streamline of the unperturbed system. As $\Omega(\psi)$, being of order 1 in this analysis, is much larger than the rate of change in $\dot{\psi}$ or $\dot{\phi}$, there are two time scales in the system: s is a fast variable while ψ and ϕ are slow variables. This is illustrated in Fig. 2 where we plot a long streamline from a single initial condition. As the trajectory quickly winds around a path resembling a closed streamline from the unperturbed flow, the azimuthal position and the stream function slowly changes.

Thus, we can simplify the description of motion by averaging (5) over a fast period to get

$$\dot{\psi} = \epsilon F(\psi, \phi), \quad \dot{\phi} = \epsilon G(\psi, \phi), \quad (6)$$

where

$$F = \frac{1}{T(\psi)} \oint (\nabla \psi \cdot \mathbf{v}_\epsilon) dt \quad G = \frac{1}{T(\psi)} \oint (\nabla \phi \cdot \mathbf{v}_\epsilon) dt. \quad (7)$$

Here \mathbf{v}_ϵ is the perturbed velocity field [the terms with ϵ in (4)] and $T(\psi) = 2\pi/\Omega(\psi)$ is the period of the unperturbed system.

Following Neishtadt *et al.* [3,17] we denote $\Phi(\psi, \phi)$ as the flux of the perturbation vector \mathbf{v}_ϵ across a surface S spanning the streamline of the unperturbed system $\Gamma_{\psi, \phi}$. This flux depends on ψ and ϕ and is independent of the choice of the spanning surface, since the flow is incompressible. Thus

$$\Phi(\psi, \phi) = \int_S \mathbf{v}_\epsilon \cdot \mathbf{n} dS, \quad (8)$$

where \mathbf{n} and dS are the unit normal on S and an area element in S . The positive direction of \mathbf{n} is defined as follows: On the surface S , there is the natural direction of rotation, specified by the unperturbed motion along its edge. The positive direction of the normal is taken to be the direction of the angular velocity of this rotation. Φ is the Hamiltonian for the average system and the adiabatic invariant (AI) of the perturbed system. Using the Stokes theorem, we can write Φ as an integral along the

curve:

$$\Phi(\psi, \phi) = \oint_{\Gamma_{\psi, \phi}} \mathbf{A} \cdot d\ell, \quad (9)$$

where $d\ell$ is the length element on $\Gamma_{\psi, \phi}$ and \mathbf{A} is the vector potential of the perturbation velocity field ($\mathbf{v}_\epsilon = \nabla \times \mathbf{A}$) and is given by

$$\begin{aligned} (A_r, A_\theta, A_\phi) &\rightarrow ((5r^4 - 3r^2) \sin \theta \sin \phi, 0, \\ &2(r^2 - r^4) \cos \phi \sin^2 \theta). \end{aligned} \quad (10)$$

Substituting (10) into (9) we obtain

$$\Phi(\psi, \phi) = \oint_{\Gamma_{\psi, \phi}} (5r^4 - 3r^2) \sin \theta \sin \phi dr. \quad (11)$$

In (11) we took into account that $d\phi = 0$ along $\Gamma_{\psi, \phi}$.

Portraits of the averaged system for $W = 2, 4, 10$ are shown in Fig. 3. The vertical axes are the values for ψ and the scale varies with W . The separatrix for the unperturbed flow (indicated in the graphs) is located at $\psi = 0$. The horizontal axis is the azimuthal location ϕ on the domain $0 < \phi < \pi$ (recall the flow is symmetric about $\phi = \pi$). The (closed) curves are lines of constant Φ where $\psi_{\Phi_{\max+}}, \psi_{\Phi_{\max-}}$ is the maximum value of the AI in the region above or below the separatrix, respectively. The closed curves represent a streamline that travels in the azimuthal direction, encounters the symmetry plane, and changes hemispheres and rotation then travels to the same symmetry plane from the other direction (see Fig. 2).

In Fig. 3(a), where $W = 2$, the separatrix intersects just a small region near the top of the plot, and below $\psi = 0$ there is a family of closed orbits that do not intersect the separatrix. In Fig. 3(b), where $W = 4$, the separatrix intersects a larger portion of the domain as we see the appearance of closed curves in the region above the separatrix whereas in Fig. 3(a) we do not. In Fig. 3(c), where $W = 10$, the separatrix intersects still a larger portion of the trajectories than in the two previous figures but, once again, we see that in the region above the separatrix for larger W there is a larger portion of the domain that contains closed curves and a decrease in the number of intersections along ϕ .

The location of the maximum Φ is important in determining stirring kinematics since the largest difference between the

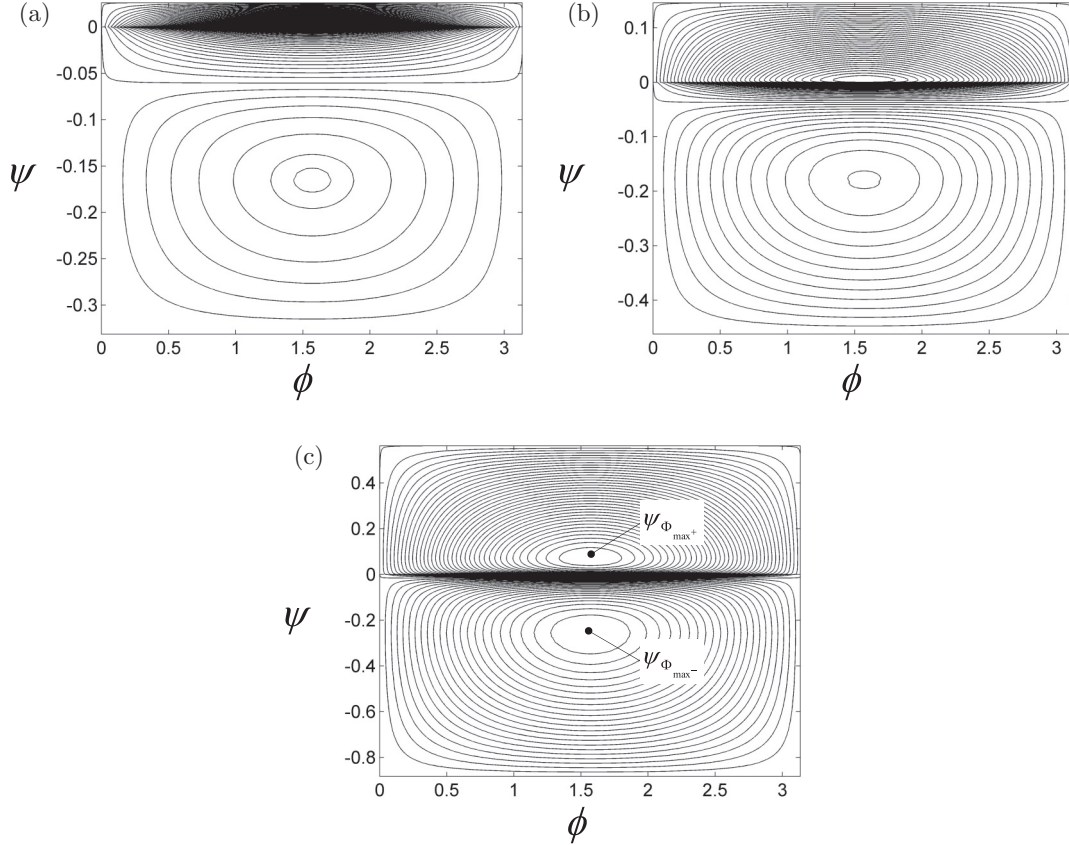


FIG. 3. Plots of ψ vs ϕ for $W =$ (a) 2, (b) 4, and (c) 10.

values above and below the separatrix yield the largest change in the AI for the trajectories that cross it. The maximum value always appears at the farthest point from the symmetry plane $\phi = \pi/2$. Shown in Fig. 4(a) is the ψ location of $\psi_{\Phi_{\max}}$ for various values of W . Figure 4(b) shows the values of Φ_{\max} versus W above and below the separatrix. There is a local minimum in the Φ_{\max} that occurs at $W = 2$ below the separatrix. Above the separatrix the value increases logarithmically for the range of W values shown in Fig. 4(b).

B. Asymptotic analysis near the separatrix

In the vicinity of the separatrix of the unperturbed flow (a horizontal plane located at $z = r \sin \theta = 1/W$ and is defined by $\psi = 0$) the frequency of fast motion, $\Omega(\psi)$, goes to 0 and the method of averaging is invalid. This is due to the fact that the separatrix consists of two fixed points, so it requires an infinite amount of time to traverse. Therefore, we expect that the value of the AI changes as a streamline crosses the separatrix.

To analyze this behavior, first we expand the expression for the AI near the separatrix (for small ψ) which yields

$$\Phi(\psi, \phi) = \sin \phi \left(\frac{1}{W^5} - \frac{1}{W^3} \right) + 2a(\phi, W)\sqrt{|\psi|} + O(\psi^2),$$

where

$$a(\phi, W) = \sin \phi \int_{1/W}^1 \frac{5r^3 - 3r}{\sqrt{(Wr - 1)(1 - r^2)}} dr.$$

Following Ref. [3], let us define the change in AI due to a single separatrix crossing as follows. Consider a segment of a perturbed streamline that crosses the separatrix once. Let M_- and M_+ be its initial and final points lying at a distance of order 1 from the separatrix. Denote using $\psi_{\pm}, \phi_{\pm}, \Phi_{\pm}$ the values of functions ψ, ϕ, Φ at the points M_{\pm} . To be specific, we suppose that the point M_- lies in the southern hemisphere ($\psi_- < 0$) and M_+ lies in the northern hemisphere ($\psi_+ > 0$). The segment resembles a plane spiral with the size of the turns slowly increasing in the southern hemisphere (before the crossing) and slowly decreasing in the northern hemisphere (after the crossing). The objective is to calculate $\Delta \Phi = \Phi_+ - \Phi_-$ for small ϵ .

To numerate the turns of the spiral between M_- and M_+ , on each turn of the spiral mark the point, where $r=0, r > 1/W$ (the closest to the surface of the sphere point of the turn). We shall use notation M_k to represent these points. We enumerate these points so $k \leq 0$ for $\psi < 0$ and $k > 0$ for $\psi > 0$; increasing $|k|$ corresponds to receding from the separatrix. Thus, M_0 is the last of the points M_k prior to the separatrix crossing, and M_1 is the first of them after the crossing. The turn of the streamline between M_{k-1} and M_k is called the k th turn and denoted by γ_k .

On each turn γ_k in the first approximation and the value of ψ changes by the same quantity

$$\Theta = \psi_k - \psi_{k-1} = \cos \phi_0 \left(\frac{1}{W^5} - \frac{1}{W^3} \right) + O(\epsilon).$$

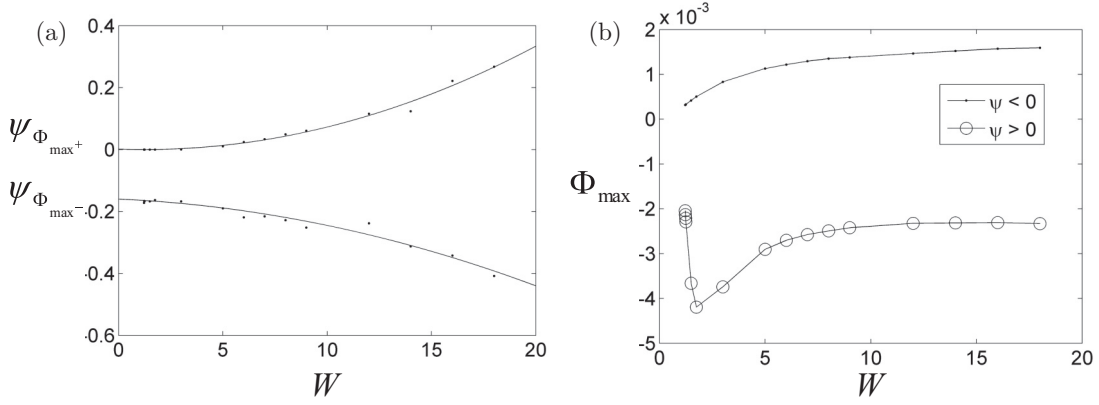


FIG. 4. (a) Plots of $\psi_{\Phi_{\max^+}}$ (northern hemisphere) and $\psi_{\Phi_{\max^-}}$ (southern hemisphere) vs W . (b) Plots of Φ_{\max} vs W for the southern $\psi < 0$ and northern $\psi > 0$ hemispheres.

Now we can write $\Delta\Phi$ as a sum over changes in Φ on a single turn γ_k . This derivation is very similar to the one presented in Ref. [3] and we do not repeat it here. We finally get:

$$\Delta\Phi(\phi_0, \xi) = \sqrt{\frac{\epsilon|\Theta|}{\pi}} a(W, \phi_0) f(\xi), \quad (12)$$

where

$$f(\xi) = \int_0^\infty \sqrt{\tau} \frac{e^{-\xi\tau} - e^{-(1-\xi)\tau}}{1 - e^{-\tau}} d\tau.$$

In (12), ψ_0 and ϕ_0 are the values of ψ and ϕ at the last point M before the crossings, namely at M_0 . The quantity $\xi = \psi_0/(\epsilon|\Theta|) \in (0,1)$ defines the crossing. The value of ξ is very sensitive to small changes in initial conditions: $O(\epsilon)$ changes in ψ_- and ϕ_- may lead to large changes of order of 1 in ξ . Therefore for multiple crossings ξ can be treated as a random variable uniformly distributed on $(0,1)$ [3,17]. Consequently, $\Delta\Phi$ is also a random variable. In the Fig. 5(a) inset we show a plot of the integral in (12) versus ξ . The change in the AI is singular at $\xi = 0$ and $\xi = 1$. It follows from (12)

that the ensemble average value of $\Delta\Phi$ is zero:

$$\langle \Delta\Phi \rangle = \int_0^1 \Delta\Phi(\xi) d\xi = 0. \quad (13)$$

The comparison of the analytical predictions of the change in AI given by (12) with the results of numerical simulations of (4) for different W are shown in Fig. 5 as a log-log plot of $\Delta\Phi$ vs ϵ for $\xi = 0.3$, $\phi_0 = \pi/4$, and $W = 2$ and 4. Both plots show an increase in the change of $\Delta\Phi$ as the tilt angle, ϵ , is increased. Overall, the change in the AI for $W = 4$ is slightly larger than with $W = 2$. Both plots show that the numerical data and the analytical results are in good agreement.

C. Long-time dynamics

There are two types of the streamlines. Some intersect the separatrix and some do not. Portraits of the averaged system of equations reveal AI trajectories that cross the separatrix surface and AI trajectories that orbit closed trajectories. We qualitatively show that the closed trajectories of the averaged system are KAM surfaces which are the ordered regions that coexist with chaotic regions.

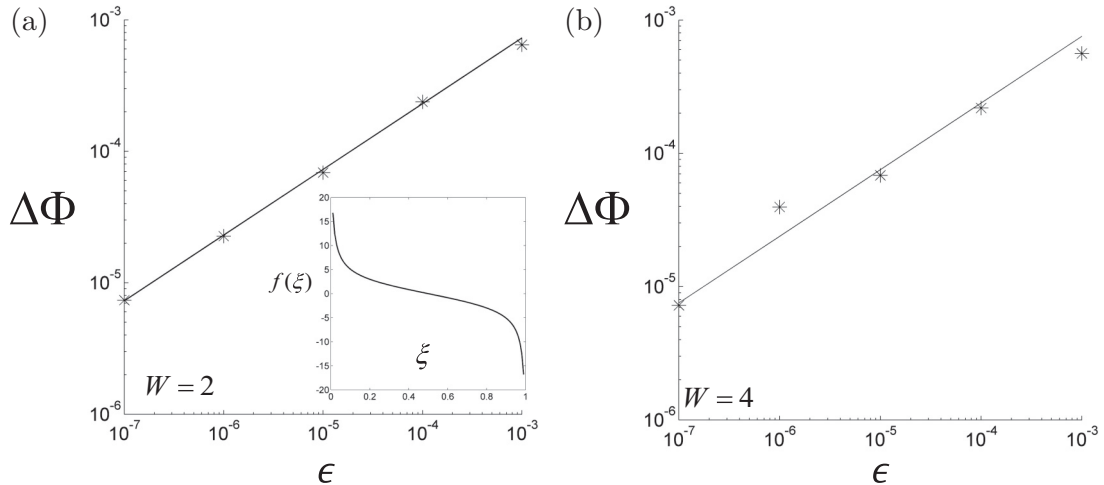


FIG. 5. Log-log plot of the change in the adiabatic invariant Φ vs ϵ for (a) $W = 2$ and (b) $W = 4$. Straight line is the analytical result.

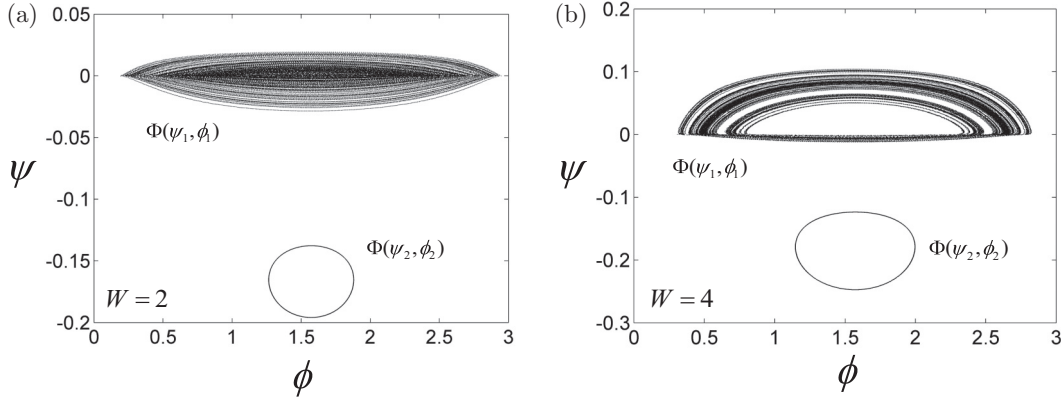


FIG. 6. Trajectory plots (ψ vs ϕ) of multiple crossing in the vicinity of, and away from, the separatrix of the unperturbed flow for $W =$ (a) 2 and (b) 4.

In the previous section we showed that crossing the SUF leads to quasirandom jumps in the AI. We were able to expand the AI in the region near the SUF to an accuracy of $O(\epsilon)$ and estimate the AI jump. There was good agreement between the averaged system and the full system for the AI jump versus ϵ . We now discuss the situation when the AI crosses the separatrix more than once.

For the averaged system the AI (Φ) is conserved as it crosses the separatrix. This is not the case though for the exact system where it is shown to suffer a quasirandom jump in the AI by an amount $\sqrt{\epsilon}$ an $O(\epsilon)$ away from the SUF as shown in Fig. 6. Here in Fig. 6 we show plots of the exact system in term of the slow variables ψ versus ϕ for $\epsilon = 0.0001$ and $W = 2$ and 4 with two separate initial conditions in each plot. The regions far from the separatrix never suffer the quasirandom jumps in the AI that are experienced by the trajectories that do.

Furthermore, it was shown in Refs. [3,21] that the characteristic time of mixing is $t \sim \epsilon^{-2}$ for bounded three-dimensional systems. In Fig. 7 we plot on a semilog scale the maximum value of the AI for four difference values of ϵ as indicated in the graph. The initial conditions are chosen so the trajectories cross the AI but with initial Φ values that are close to zero. Although we were not able to start from $\Phi = 0$ the values are close enough to show relative behavior where the diffusion of

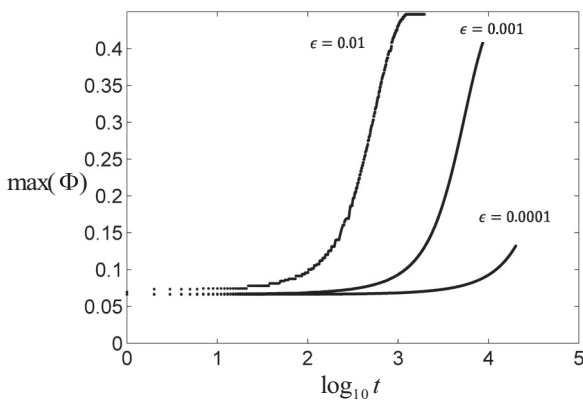


FIG. 7. Plot illustrating the long-time evolution of the adiabatic invariant Φ versus $\log_{10} t$ for $\epsilon = 0.01, 0.001,$ and 0.0001 . The initial condition is chosen so $\Phi \approx 0$.

the AI (where we simply use the approximate time required to reach the maximum) scales more like $t \sim \epsilon^{-4/3}$. We believe that better agreement with theory [3,17,21] would be achieved for smaller initial Φ .

Following Ref. [21], the long-time mixing due to multiple separatrix crossings can be quantitatively described in terms of the probability distribution function $\Psi = \Psi(\Phi, N): d\Psi$, which represents the number of streamlines whose values of adiabatic invariant are in $(\Phi - d\Phi/2, \Phi + d\Phi/2)$ after N periods of slow motion (i.e., $2N$ separatrix crossings). This method, which relates the spreading (diffusion) of $\Psi = \Psi(\Phi, N)$ to the solution of a diffusion-type PDE, is described in more detail in the second part of the paper, Sec. IV E, in application to the unsteady flow. In the present setup the results are very similar to the ones presented in Ref. [21], and we do not reproduce them here.

IV. UNSTEADY AXISYMMETRIC FLOW

We now turn to mixing inside a drop settling with a spatially uniform unsteady electric field oriented parallel relative to the translational motion [5,6]. Instead of an autonomous three-dimensional flow discussed in the previous section, we get a nonautonomous two-dimensional (axisymmetric) flow. As shown in Fig. 1, the resulting velocity field is an superposition of Taylor and Hadamard-Rybczynski circulations due to the electric field and settling, respectively. Mixing in this flow is driven by time-periodic perturbations of the base Taylor circulation yielding $\psi = \psi_B + W(t)\psi_E$, where

$$W(t) = W_1 + W_2 \cos(\epsilon t). \tag{14}$$

Parameter ϵ appearing here is frequency ω normalized by the residence time: $\epsilon = 2a\omega(1 + \lambda)/(U\pi)$, see Ref. [6]. For the sake of definiteness, we assume that $W_1, W_2 > 0$. We also assume that the direction of the Taylor circulation does not change sign, i.e., $W_1 \geq W_2$. One can see that the value of W changes varies over time $2\pi/\epsilon$. Thus, characteristic values of the time t are of order of $1/\epsilon$.

To illustrate two time scales in this problem, it is convenient to denote $\epsilon t \equiv \phi$ (an analog of the azimuthal angle in the 3D case) and augment (3) with $\dot{\phi} = \epsilon$. Thus the equations of

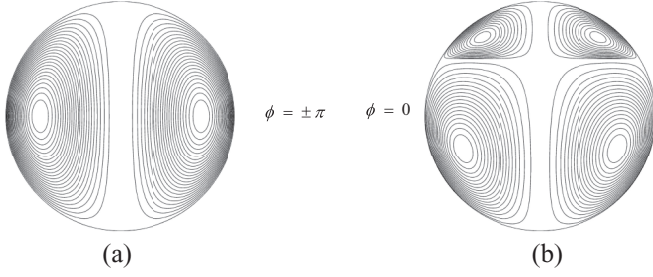


FIG. 8. Typical unperturbed streamlines for different values of the slow phase ϕ ; $W_1 = 2$, $W_2 = 2$. (a) $\phi = \pm\pi$, only one elliptic point is present on each side of the vertical axis; (b) $\phi = 0$, two elliptic points are present.

motion can be written as

$$\begin{aligned} \dot{r} &= 2(r^2 - 1)\cos\theta + W_1(r - r^3)(3\cos\theta - 1) \\ &\quad + W_2\cos\phi(r - r^3)(3\cos\theta - 1) \\ \dot{\theta} &= \frac{1}{r}(2 - 4r^2)\sin\theta + W_1(5r^2 - 3)\sin\theta\cos\theta \\ &\quad + W_2\cos\phi(5r^2 - 3)\sin\theta\cos\theta \\ \dot{\phi} &= \epsilon. \end{aligned} \quad (15)$$

In this modified system, different moments of (slow) time correspond to different values of ϕ . Notice that the equation $\dot{\phi} = \epsilon$ does not have a singularity near the vertical axis ($\theta = 0$).

A. Unperturbed system

The unperturbed system corresponds to fixing the value of W defined in (14) or, equivalently, fixing the value of ϕ in (15). Naturally, the shape of the instantaneous unperturbed streamlines differ for different values of W (or ϕ). Note that just setting $\epsilon = 0$ is misleading: In that case we get $W = W_1$, which is not what we want. The setup becomes clearer if we consider ϕ and t to be separate variables, related by the last line in (15). Different trajectories of the unperturbed system will correspond to different, but fixed, values of ϕ .

The unperturbed system (with fixed value of ϕ or W) has the following fixed points. Regardless of the value of W_1 and W_2 , there are elliptic fixed points in the southern hemisphere (below the separatrix), see Fig. 8. For $W(\phi) < 1$, the only other fixed points are the hyperbolic fixed points at the poles of the sphere [Fig. 8(a)]. For $W(\phi) > 1$, there are additional fixed points: the elliptic fixed point in the northern hemisphere and hyperbolic fixed points on the surface of the sphere and on the axis of the sphere. The horizontal plane passing through those hyperbolic points,

$$W(\epsilon t) r \cos\theta = 1,$$

is the separatrix. On it the stream function, ψ , is equal to zero, see (2). The separatrix penetrates the drop at least for a part of the slow period when $W(\epsilon t) > 1$, which happens if $W_1 + W_2 > 1$. In terms of $z = r \cos\theta$ (the vertical coordinate in Fig. 1 or Fig. 8), the separatrix is moving between $z_{\min} = 1/(W_1 + W_2)$ and $z_{\max} = 1/(W_1 - W_2)$. If $z_{\min} > 1$, the separatrix is always outside the drop, and in that regime the regular domain covers the entire drop. If $z_{\min} < 1$ and

$z_{\max} \leq 1$, then the separatrix is always inside the drop. If $z_{\min} < 1$ and $z_{\max} > 1$, then the separatrix is outside for a part of the slow period.

B. Averaged system and the adiabatic invariants

In the case $\epsilon \ll 1$ there is a separation of time scales: r and θ are fast variables while ψ and ϵt are slow variables. Therefore, in the first approximation, we can average the equations of motion over the fast time scale. The quantity $\tilde{\Phi}^0$, which is the normalized-by- 2π area surrounded by a closed curve $\Gamma_{\psi,\phi}$ of the unperturbed system, is an integral of the averaged system and an adiabatic invariant of the exact system (see, e.g., Ref. [3]). The superscript “0” indicates that $\tilde{\Phi}^0$ is the zeroth-order approximation to the AI. Note that if we consider the augmented system (with $\phi = \epsilon t$ and $\dot{\phi} = \epsilon$), then $2\pi\tilde{\Phi}^0$ has exactly the same meaning, the flux of perturbation [$v_\epsilon = (v_r, v_\theta, v_\phi) = (0, 0, 1)$] through a surface spanned over the closed curve of the unperturbed system, as in the previous section. Using a vector potential $\mathbf{A}_\epsilon = (r^2 \cos\theta, 0, 0)$ we can write $\tilde{\Phi}^0$ as

$$\tilde{\Phi}^0(\psi, \phi) = \frac{1}{2\pi} \oint r^2 \cos\theta dr = \frac{1}{2\pi} \int_T r^2 \cos\theta \left(\frac{dr}{dt} \right) dt. \quad (16)$$

Here $T = T(\psi, \phi)$ is the period on $\Gamma_{\psi,\phi}$. Direct calculations indicate that $2\pi\tilde{\Phi}^0$ has a step of the magnitude $2/3$ on the separatrix. To avoid that discontinuity, we redefine $\tilde{\Phi}^0(\psi, \phi)$ as

$$2\pi\Phi^0 = 2\pi\tilde{\Phi}^0 - 1/3 \operatorname{sgn}(\psi). \quad (17)$$

The quantity Φ^0 defined by (16) and (17) has the maximum value $2\pi\Phi_{\max}^0 = 1/3$ at the elliptic fixed point in the southern hemisphere (below the separatrix), see Fig. 8. The minimum value, $2\pi\Phi_{\min}^0 = -1/3$ is achieved either at the elliptic point in the northern hemisphere (above the separatrix), if that point exists, see Fig. 8(a), or at the streamline that covers the whole semicircle, if the northern elliptic points are outside the drop, see Fig. 8(b).

In the exact system the value of Φ^0 oscillates with the amplitude of order ϵ over a period of fast motion. In the 3D case, considered in the previous section, this accuracy was sufficient (recall that the jumps in the adiabatic invariant at the separatrix were of order of $\sqrt{\epsilon} \gg \epsilon$). In the time-dependent case, it was shown in Refs. [15,16] that for a proper description we need to introduce an *improved adiabatic invariant* by adding a correction term to Φ^0 to reduce the oscillations. Following Ref. [15], we have for the improved adiabatic invariant

$$\Phi(\phi, \psi) = \Phi^0(\phi, \psi) + \epsilon u(\psi), \quad (18)$$

where the correction u is given by

$$2\pi u(\psi) = \frac{1}{\epsilon} \int_T \left(\frac{T}{2} - t \right) \frac{\partial \psi}{\partial t} dt. \quad (19)$$

The integral in (19) is taken along a closed trajectory of the unperturbed system [given by (15) with $W = \text{const}$] that passes through a given point. Note that as $\partial\psi/\partial t \sim \epsilon$, characteristic values of ϵu are of order ϵ . It was shown in Ref. [15] that, far from the separatrix, Φ oscillates with the amplitude of order ϵ^2 . A typical evolution of the original,

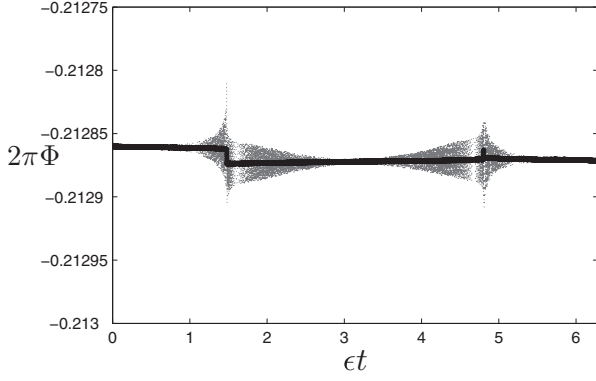


FIG. 9. Evolution of the adiabatic invariants. Dash: The zeroth order AI, Φ^0 ; solid: improved AI, Φ . A significant difference in the magnitude of oscillations is clearly visible.

Φ^0 , and improved, Φ , adiabatic invariants is presented in Fig. 9. One can see that the oscillations of Φ is by orders of magnitude smaller than the oscillations of Φ^0 .

C. Separatrix crossings and the change of adiabatic invariant

The averaging method is not valid near the separatrix surface. Thus we need to apply additional considerations to describe the dynamics in that region.

Following Refs. [3,17] and Sec. III, let us define the change in AI due to a single separatrix crossing as follows. Identical to Sec. III, consider a segment of a perturbed streamline that crosses the separatrix once. Let M_- and M_+ be its initial and final points lying at a distance of order 1 from the separatrix. Denote by ψ_{\pm} , ϕ_{\pm} , Φ_{\pm} the values of functions ψ , ϕ , Φ at the points M_{\pm} . To be specific, we suppose that the point M_- lies in the southern hemisphere ($\psi_- < 0$) and M_+ lies in the northern hemisphere ($\psi_+ > 0$). The segment almost looks like a plane spiral with the size of the turns slowly increasing in the northern hemisphere (before the crossing) and slowly decreasing in the southern hemisphere (after the crossing). The objective is to calculate $\Delta\Phi = \Phi_+ - \Phi_-$ for small ϵ .

To numerate the turns of the spiral between M_- and M_+ , on each turn of the spiral we mark the point where $\dot{r} = 0, r > 1/W$ (the closest to the surface of the sphere point of the turn in terms of r). We use the notation M_k to represent these points, enumerating them so $k \leq 0$ for $\psi < 0$ and $k > 0$ for $\psi > 0$; increasing $|k|$ corresponds to receding from the separatrix. Thus, M_0 is the last of the points M_k prior to the separatrix crossing, and M_1 is the first of them after the crossing. The turn of the streamline between M_{k-1} and M_k is called the k th turn and denoted by γ_k . The location of some of the points M_k immediately near S is shown in Fig. 10.

For the parts of the streamline that are close to the separatrix (in other words, for small values of ψ) the adiabatic invariant Φ^0 can be expressed as

$$\Phi^0(\phi, \psi) = \Phi_0(\phi) + \Phi_1(\phi, \psi). \tag{20}$$

In (20), $\Phi_0 = \Phi_0(\phi)$ is the value of Φ^0 at S :

$$2\pi\Phi_0 = \frac{1}{6W_*^3} - \frac{1}{2W_*}, \tag{21}$$

where $W_* = W_1 + W_2 \cos \phi_*$ is the value of W at the moment of crossing.

The expression for $\Phi_1(\phi, \psi)$ can be found directly as a flux of perturbation through a narrow strip between the separatrix contour and $\Gamma_{\psi, \phi}$. However, there is a simpler way. It was shown in Refs. [3,17] that adiabatic invariant $\Phi^0(\phi, \psi)$ is a Hamiltonian for the averaged system:

$$\dot{\psi} = \frac{1}{T(\phi, \psi)} \frac{\partial \Phi^0}{\partial \phi}, \quad \dot{\phi} = -\frac{1}{T(\phi, \psi)} \frac{\partial \Phi^0}{\partial \psi}. \tag{22}$$

Thus, we can get the expression for $\Phi^0(\phi, \psi)$ by computing the change in ϕ and ψ over one period.

The change in the slow time, ϵt , equals ϵ times the period of the unperturbed system, T :

$$\Delta\phi = \phi_k - \phi_{k-1} = \epsilon T.$$

In the vicinity of the separatrix surface the period T has a logarithmic singularity that in the leading order can be

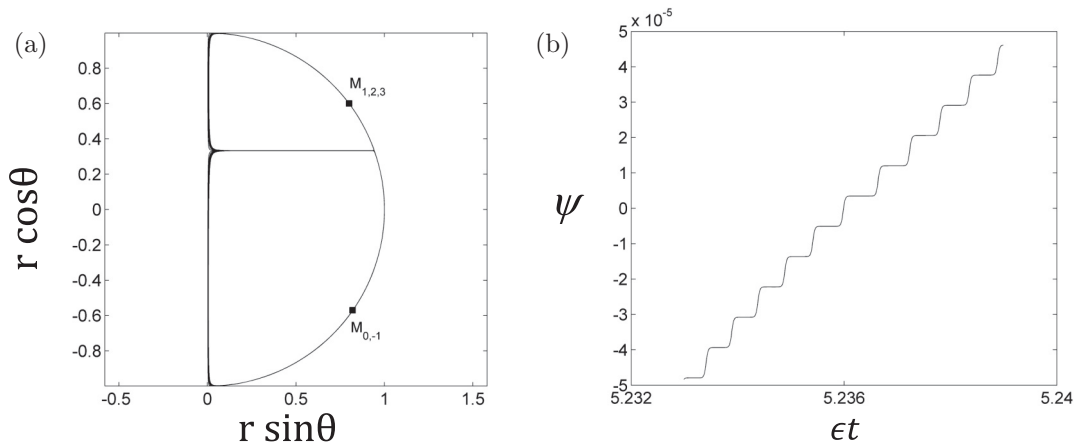


FIG. 10. Numerical simulation of a particle trajectory near the separatrix for $W_1 = 2, W_2 = 2, \epsilon = 10^{-4}$: (a) Projection on the fast, $(r \cos \theta, r \sin \theta)$ plane and (b) the corresponding averaged system [projection on the slow, $(\epsilon t, \psi)$ plane].

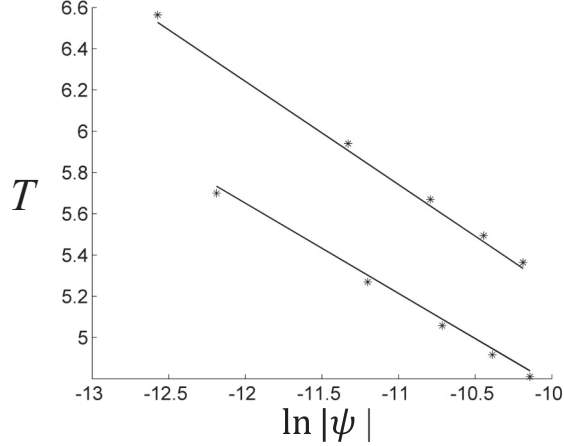


FIG. 11. Period T versus $\ln|\psi|$ for $W_1 = 2, W_2 = 2, \epsilon = 10^{-4}$. The stars are obtained from numerical simulations of the unperturbed system, and the solid lines correspond to (23) and (24), with b_{\pm} computed numerically using (25) for the rightmost point. Bottom: Before the separatrix crossing (T_-); top: after the separatrix crossing (T_+).

written as:

$$T_{\pm} = A_{\pm}(\phi) \ln|\psi| + b_{\pm}(\phi). \quad (23)$$

Note that both A and b differ before and after the crossing, in other words, for $\psi < 0$ and $\psi > 0$. Direct calculation yields

$$A_{-} = -\frac{1}{W_* + 1} \left(\frac{W_*}{W_* - 1} + \frac{1}{4} \right), \quad (24)$$

$$A_{+} = -\frac{1}{W_* - 1} \left(\frac{W_*}{W_* + 1} + \frac{1}{4} \right).$$

In (24) and below, the plus or minus subscripts correspond to the sign of ψ . The analytical expressions for b_{\pm} can be written as well, but they are quite complex and it is easier to compute them numerically using direct definition (23):

$$b = T(\psi = \text{const}, W = \text{const}) - A \ln|\psi|. \quad (25)$$

The change of unperturbed period of a perturbed particle trajectory is presented in Fig. 11. The analytical expression of unperturbed period (23) with b_{\pm} obtained by (25) shows a good agreement with the results of numerical simulations. It follows from (22) that

$$\Delta\phi = -\frac{\partial\Phi^0}{\partial\psi} = -\frac{\partial\Phi_1}{\partial\psi},$$

and we obtain the expression for $\Phi^0(\phi, \psi)$:

$$2\pi\Phi^0 = 2\pi\Phi_0 + A_{\pm}(\psi \ln|\psi| - \psi) + b_{\pm}\psi + o(\psi). \quad (26)$$

The change of ψ between M_k and M_{k-1} is in the leading order given by

$$\begin{aligned} \Delta\psi &= \psi_k - \psi_{k-1} = \int_T \frac{\partial\psi}{\partial t} dt \\ &= \epsilon W_2 \sin(\phi_*) \frac{1}{2W_*^2} \left(\frac{1}{W_*^2} - 1 \right) \equiv \epsilon\Theta. \end{aligned}$$

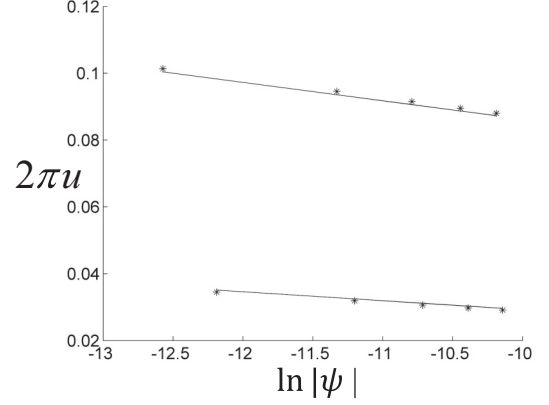


FIG. 12. The values of u_{\pm} computed at the points M_k versus $\ln|\psi|$ for $W_1 = 2, W_2 = 2, \epsilon = 10^{-4}$. The stars are the results of the numerical computation, and the solid line corresponds to (27) with d_{\pm} computed using (27) for the rightmost point. Bottom: Before separatrix crossing (u_-); top: after separatrix crossing (u_+).

Comparing the above expression with $\partial\Phi_0/\partial\phi$, one can see that (22) is satisfied.

Similarly, we can expand the function u from (19) at the points M_k to get

$$2\pi u_{\pm} = \Theta \left(-\frac{1}{8} \frac{1}{W_* \mp 1} \ln|\psi| + d_{\pm} \right), \quad (27)$$

with the values of d_{\pm} to be computed numerically using (27) as a definition. Typical comparison is presented in Fig. 12.

Thus, we can readily apply a general formula from [15] to get

$$\begin{aligned} \Delta\Phi &= \frac{\epsilon\Theta}{2\pi} \left\{ \frac{A_- - A_+}{2} (1 - 2\xi) \ln|\epsilon\Theta| + \frac{A_- + A_+}{2} \ln 2\pi \right. \\ &\quad - [A_+ \ln \Gamma(\xi) + A_- \ln \Gamma(1 - \xi)] \\ &\quad \left. + [b_+(1 - \xi) + b_- \xi] + (d_- - d_+) \right\}. \quad (28) \end{aligned}$$

Note that in (28) the quantities $b_{\pm}, d_{\pm}, A_{\pm}$, and Θ are functions of the slow time and must be computed at the moment of crossing, $\epsilon t = \epsilon t_*$. The quantity $\xi = \psi_s/\epsilon\Theta \in (0, 1)$ defines the location of crossing: ψ_s denotes the value of ψ at the last point M before crossing (M_0) for a crossing from south to north or the first point M after crossing (M_1) for a crossing from north to south. The value of ξ is very sensitive to small changes in initial conditions: $O(\epsilon)$ changes in ψ_s and ϕ_* may lead to large changes, of order 1, in ξ .

The comparison of the analytical predictions of the change in Φ given by (28) with the results of direct numerical simulations of (15) for different ξ are shown in Fig. 13 for $\epsilon = 10^{-4}$. The dots are results of direct numerical simulations while the solid curve is the plot of (28). Figure 13 shows that the numerical data and the analytical results are in a good agreement. There are logarithmic singularities in $\Delta\Phi$ at $\xi = 0$ and $\xi = 1$. In reality, expression (28) becomes invalid for very small values of ξ or $1 - \xi$. It was shown in Ref. [22] that corrections must be applied to (28) if $\xi < \epsilon$ or $1 - \xi < \epsilon$.

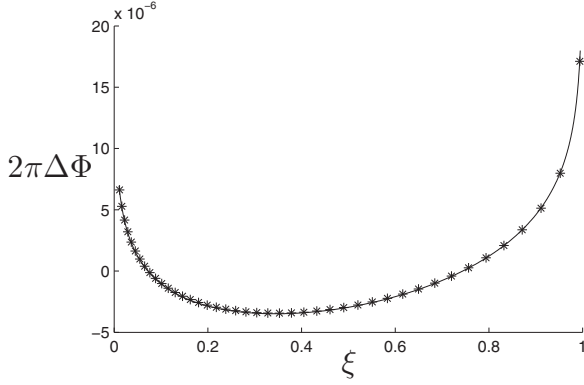


FIG. 13. The change in the adiabatic invariant $\Delta\Phi(\xi)$ for $W_1 = 2$, $W_2 = 2$, $\phi_* = 5\pi/3$, and $\epsilon = 10^{-4}$. The solid line corresponds to (28), the stars are the values obtained by numerically integrating exact system (15).

D. Long-time dynamics

As the motion of the separatrix plane forces some streamline to cross it, it was shown in our previous publications (see, e.g., Ref. [3]) that the chaotic and regular domains are filled with the streamlines that do and do not cross the separatrix, respectively. The respective location of the regular and chaotic domains depends on the relation between the values of W_1 and W_2 . (Recall that for the sake of definiteness we assumed that $0 < W_2 \leq W_1$).

The regular domain near the elliptic fixed points in the southern hemisphere is always present (independently of the values of W_1 and W_2 as long as $0 < W_2 \leq W_1$). The regular domain near the elliptic fixed points in the northern hemisphere is present only if those fixed points exist for all the values of ϕ , in other words, for $W_2 \leq W_1 - 1$. The larger the value of W_2 , the smaller the regular domain.

The division of the drop between the regular and chaotic domains is illustrated in Fig. 14. In Fig. 14(a), the regular domain exits in the northern hemisphere [above the curve defined by the condition $\psi = 0$ at $\phi = \pm\pi$, or $\Phi = \Phi_{nb}^{(0)} = \Phi^0(0, \pi)$] and in the southern hemisphere [below the curve defined by the condition $\psi = 0$ at $\phi = 0$, or $\Phi = \Phi_{sb}^{(0)} = \Phi^0(0, 0)$]. The expressions for $\Phi_{nb}^{(0)}$ and $\Phi_{sb}^{(0)}$ are given by

(21) with $W_* = W_1 - W_2$ and $W_* = W_1 + W_2$, respectively. In Fig. 14(b), the regular domain exits in the southern hemisphere only [below the curve defined by the condition $\psi = 0$ at $\phi = 0$ or $\Phi = \Phi_{sb}^{(0)} = \Phi^0(0, 0)$]. The expression for $\Phi_{sb}^{(0)}$ is given by (21) with $W_* = W_1 + W_2$.

To describe the overall mixing, we need to discuss the evolution of the system over the times of order $\sim 1/\epsilon^3$. Consider streamlines that cross the separatrix many times. Upon every crossing, the value of the improved adiabatic invariant changes according to (28). As ξ is a random variable, the change of AI due to a separatrix crossing can be viewed a 1D random walk (see, e.g., Refs. [3,22]) with the characteristic step size given by (28).

Following Ref. [23], the long-time mixing can be described in terms of the probability distribution function $\Psi = \Psi(\Phi, N)$: The number of streamlines whose values of adiabatic invariant are in $(\Phi - d\Phi/2, \Phi + d\Phi/2)$ after N periods of slow motion is given by $\Psi(\Phi, N)d\Phi$. During every period of the slow motion, $T_{\text{slow}} = 2\pi/\epsilon$, streamlines inside the chaotic domain (see Sec. IV B) cross the separatrix twice. Recall that on every single crossing a characteristic change in AI is small. Therefore, the consecutive crossings occur at approximately the same location in terms of the separatrix (i.e., at the same value of W_*). By combining two successive crossings during every period of slow motion, we can describe the long-term diffusion of the adiabatic invariant with a 1D nonlinear diffusion equation:

$$\frac{\partial \Psi}{\partial N} = \frac{\partial}{\partial \Phi} \left[D(\Phi) \frac{\partial \Psi}{\partial \Phi} \right]. \tag{29}$$

Here $D(\Phi)$ is the diffusion coefficient, which is discussed next.

For any random walk, the diffusion coefficient is equal to one half of the second moment of the corresponding distribution of the magnitude of a single step. Thus, from $\Delta\Phi$ at a single separatrix crossing we obtain

$$D_1(\Phi) = \frac{1}{2} \int_0^1 [\Delta\Phi(\xi) - \langle \Delta\Phi \rangle]^2 d\xi, \tag{30}$$

where $\langle \Delta\Phi \rangle = \int_0^1 \Delta\Phi(\xi) d\xi$, is the average of $\Delta\Phi$ for one crossing. Since we combine two successive crossings in (29),

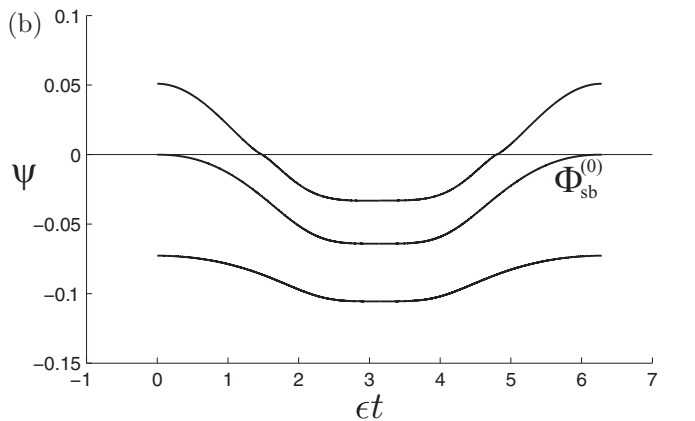
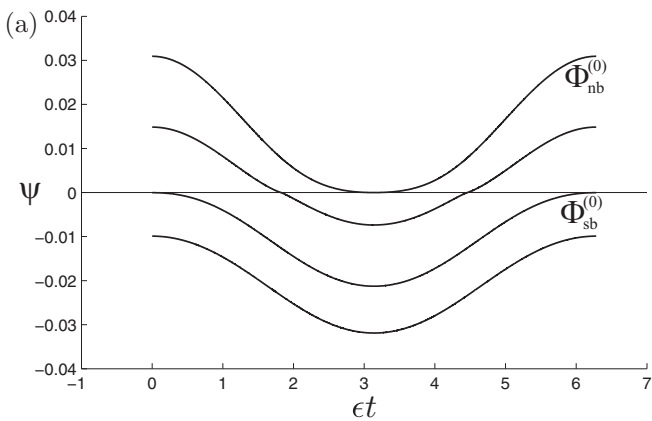


FIG. 14. Phase portraits on the slow plane: regular and chaotic domains. (a) $W_1 = 2, W_2 = 0.5 < W_1 - 1$; (b) $W_1 = 2, W_2 = 2 > W_1 - 1$. The north [in panel (a)] and the south (in both panels) bounds of the chaotic domain are indicated.

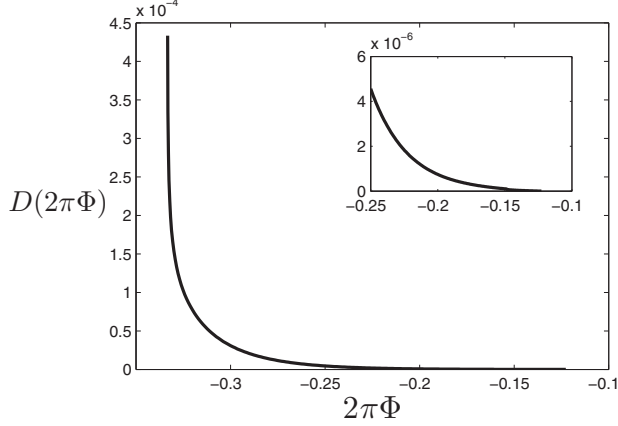


FIG. 15. Diffusion coefficient D [see (31)] as a function of $2\pi\Phi$ for $W_1 = 2$, $W_2 = 2$, $\epsilon = 10^{-2}$.

the total diffusion coefficient, $D(\Phi)$, is twice as large as $D_1(\Phi)$:

$$D(\Phi) = 2D_1(\Phi). \quad (31)$$

We performed a set of numerical experiments of (15) and compared those results to the theoretical results obtained using (29). As the mixing process occurs over a long time scale [of order $O(1/\epsilon^3)$], a relatively large value of the dimensionless frequency for the slow motion, $\epsilon = 10^{-2}$, was used for all computations discussed in the current section. For this value of ϵ , approximate expression (28) is still valid, but is not as accurate as it would be for smaller values of ϵ . The other parameters were $W_1 = 2$ and $W_2 = 2$, the same values used in the previous sections. For this particular set of W_1 and W_2 values, the range of W_* for the occurrence of separatrix crossing (i.e., the presence of separatrix inside the droplet) is $W_* \in [1, 4]$. By substituting this range of W_* into (21), the range of the adiabatic invariant of the streamlines inside the chaotic domain is approximately $2\pi\Phi \in [-1/3, -0.1224]$.

A plot of the diffusion coefficient defined by (30) and (31) is shown in Fig. 15. Note that $D(2\pi\Phi)$ is presented for the convenience of presentation. The value of D has a logarithmic singularity at $2\pi\Phi = -1/3$, at which value trajectories come to the separatrix at the hyperbolic fixed point in the northern hemisphere. On the other side of the plot, the diffusion coefficient drastically decreases as Φ approaches $2\pi\Phi \approx -0.1224$, which is the interface between the chaotic and regular domains.

For the numerical experiments, 600 initial conditions were evenly distributed inside a small box ($[r \cos \theta] \times [r \sin \theta] = [0.6 - \epsilon, 0.6 + \epsilon] \times [0.25 - \epsilon, 0.25 + \epsilon]$). Tracers were released from those initial conditions and tracked for 1500 periods of the slow motion. Initially the tracers have a very small variance in the values for the AI. The evolution of $\Psi(\Phi, N)$ for those tracers are shown as histograms in Fig. 16. The histograms are compared with solutions of diffusion equation (29) under the following initial and boundary conditions: An initial distribution possessed the same values of first and second moment as the numerical experiment at $N = 0$ [Fig. 16(a)] and flux-free boundary conditions were applied at the boundaries of the chaotic domain [Fig. 16(b)]. Those solutions are shown in Fig. 16 with solid lines. The evolution of first and second moments of both numerical and theoretical $\Psi(\Phi, N)$ is demonstrated in Fig. 17. One can see that properties of the long-time mixing considered here are accurately captured by diffusion equation (29).

V. DISCUSSION

The averaged system corresponding to the steady three-dimensional flow retains much of the features of the unperturbed flow for $W > 1$ (the value must be greater than 1 for the separatrix of the unperturbed flow to appear). The plots of the equations of motion using the slow variables, ψ versus ϕ , reveal an elliptic point where the AI is a maximum. The

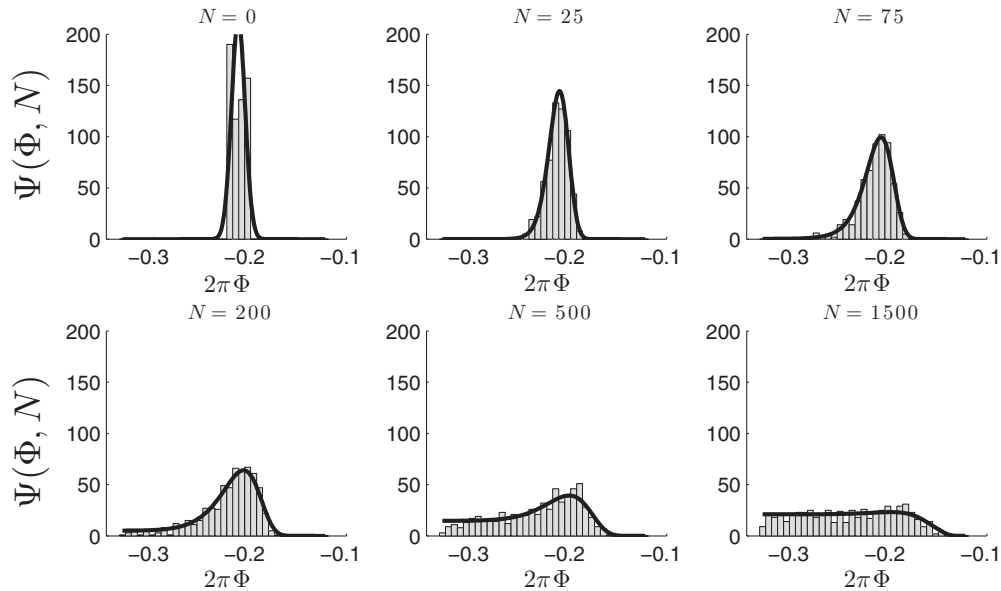


FIG. 16. Evolution of $\Psi(\Phi, N)$ for 600 particle trajectories for $W_1 = 2$, $W_2 = 2$, $\epsilon = 10^{-2}$. Histograms: numerical; solid lines: solutions to (29).

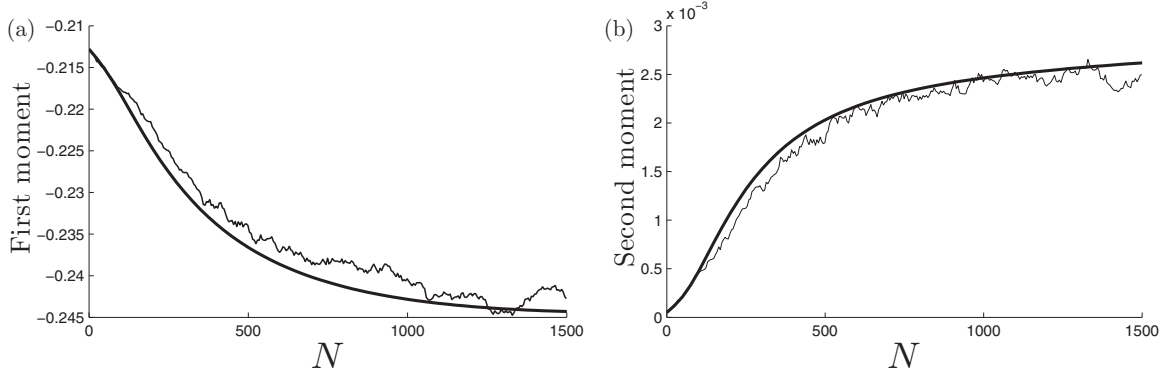


FIG. 17. Evolution of the first (a) and second (b) moment of $\Psi(\Phi, N)$ shown in Fig. 16. Solid line: numerical; bold line: theoretical.

location of the maximum AI goes like

$$\psi_{\Phi_{\max}^+} = 0.00095W^2 - 0.0024W + 0.0016$$

and

$$\psi_{\Phi_{\max}^-} = -0.00055W^2 - 0.003W - 0.16$$

in the northern and southern hemispheres of the drop, respectively. The value for Φ_{\max} increases nearly logarithmically in the northern hemisphere while there is a minimum in the southern hemisphere at approximately $W = 2$ (see Fig. 3). Therefore, there is a local maximum change in Φ_{\max} between the northern and southern hemispheres of the averaged systems for $W = 2$. This value also corresponds to a maximum in the stirred volume computed by Ward and Homsy [9]. These authors estimated the maximum stirred volume by integrating the three-dimensional steady flow equations assuming a fluid element travels along a trajectory with finite volume. The computed stirred volumes were consistently higher for $W = 2$ independent of α when compared to smaller and large values of W . This seems to confirm that the average system analysis can provide useful information for optimizing stirring, especially in steady three-dimensional flows without the need to calculate trajectories with different initial position for long periods of time.

This should not be confused, though, with the change in the adiabatic invariant for trajectories that cross the separatrix, see Fig. 5, where it was shown that the change in $\Delta\Phi$ actually increases with an increase in ϵ or, equivalently, the tilt angle α . Larger values correspond to larger jumps in the AI but not necessarily better stirring. Recall that the slow variable plots shown in Fig. 3 show the formation of larger closed Φ domain in the northern hemisphere for larger W .

In the perturbation analysis of the unsteady flow, a small value $\epsilon \sim 10^{-4}$ was used. While values that small cannot be realized in experiments, they are necessary for the described phenomena to manifest itself. Thus, we can say that the present discussion is inspired by the experiments rather than is performed to match experiments that were performed at higher modulation frequencies [6]. But the data do seem to confirm their results for the stirred volume versus modulation frequency. There these authors showed that at low modulation frequencies there was an asymptotic limit for the stirred cross-sectional volume that was determined by the sweep of the stagnation plane. The asymptotic limit for the percentage

of stirred volume increased with increasing sweep and scaled nearly one to one with the magnitude of the sweep. So this seems to confirm the main result for the averaged unsteady flow system, i.e., the percentage of the stirred volume is proportional to the magnitude of the distance traveled by the stagnation plane at low frequency. Furthermore, the volume swept by the separatrix is the minimum mixed volume for low frequencies. This is distinct from the global minimum which occurs at very high frequencies according to Ref. [6].

As far as the diffusion time of the AI this varied greatly between the two systems. The steady three-dimensional flow AI diffusion time scales according to $t \sim \epsilon^{-2}$ while it was $t \sim \epsilon^{-3}$ for the unsteady two-dimensional flow. The numerically calculated value for the three-dimensional system was slightly larger, separating the two even further. But the separation in time scales may be beneficial for removing KAM surfaces since there would not be any possibility of resonance generated by modulating the electric field via an unsteady three-dimensional flow generated by an unaligned electric field with an ac component.

When both time dependency and 3D perturbation are present, the overall structure is qualitatively the same as if one of the perturbations is present. As the flow is Stokes, the system is linear and the resulting flow is a superposition of the two perturbations. The fast system is essentially the same. In the slow system the value of adiabatic invariant due to two perturbations acting together is defined in the same way as for individual perturbations: as the total flux of the combined perturbation through a surface spanned on a closed curve of the fast system. The presence of the separatrix is independent of the particular type of perturbation. As the (combined) perturbation brings the trajectory to the separatrix, the value of the adiabatic invariant undergoes a jump, once again defined by the combined action of the perturbations. However, as the periodicity of the perturbations may differ, the dynamics on the slow plane becomes aperiodic. But on the long time, the PDF-based evolution equation approach remains valid for two perturbations.

VI. CONCLUSION

Here the problem of a drop translating in the presence of an electric field was studied in order to determine efficient stirring. Two stirring protocols were developed. The first

consists of perturbing a combined Hadamard-Rybczynski and Taylor circulations by misaligning the electric field with the translational motion. This results in a steady three-dimensional flow. The second protocol consists of modulating the electric field through the addition of a harmonic AC component with small frequency ϵ . The flow is still axisymmetric and the instantaneous streamlines are equal every $2\pi/\epsilon$ period.

In order to analyze the two systems a technique first introduced by Neishtadt was employed. The method involves describing the perturbations to the base flow by averaging. Two slow variables (a stream function and a polar angle) and a fast variable (motion around a streamline) are chosen as the new variables in the averaged domain. The fast variable dependence is removed by simple scaling with a period around a closed streamline of the unperturbed flow. In the slow variable domain it is possible to study the specific mechanism that leads to efficient stirring. In both systems this is caused by multiple crossing of the separatrix of the unperturbed flow which is characterized by the stagnation

plane of the Taylor circulation that is offset from the equator by the Hadamard-Rybczynski circulation. Comparisons are made between the average system and the full set of equations of motion when possible. The agreement between the two are good for the range of parameter values studied.

Future studies should include parametric spaces where averaging may not work. Also it would be useful to see if averaging can predict the behavior of an unsteady three-dimensional flow. In particular it would be useful to determine if the unsteady three-dimensional flow possess KAM regions similar to the steady three-dimensional or unsteady flow and if strategies to reduce the size of these regions can be developed with the averaging method.

ACKNOWLEDGMENT

This material is based upon work supported by the National Science Foundation under Grant No. CMMI-1362782 (F.W. and D.V.).

-
- [1] R. Kronig and J. C. Brink, On the theory of extraction from falling droplets, *Appl. Sci. Res.* **2**, 142 (1951).
 - [2] H. A. Stone, A. Nadim, and S. H. Strogatz, Chaotic streamlines inside drops immersed in steady Stokes flow, *J. Fluid Mech.* **232**, 629 (1991).
 - [3] A. I. Neishtadt, D. L. Vainshtein, and A. A. Vasiliev, Chaotic advection in a cubic Stokes flow, *Physica D* **111**, 227 (1998).
 - [4] S. M. Lee, D. J. Im, and I. S. Kang, Circulating flows inside a drop under time-periodic non-uniform electric fields, *Phys. Fluids* **12**, 1899 (2000).
 - [5] T. Ward and G. M. Homsy, Electrohydrodynamically driven chaotic mixing in a translating drop, *Phys. Fluids* **13**, 3521 (2001).
 - [6] T. Ward and G. M. Homsy, Electrohydrodynamically driven chaotic mixing in a translating drop II: Experiments, *Phys. Fluids* **15**, 2987 (2003).
 - [7] J. D. Tice, H. Song, A. D. Lyon, and R. F. Ismagilov, Formation of droplets and mixing in multiphase microfluidics at low values of the Reynolds and the capillary numbers, *Langmuir* **19**, 9127 (2003).
 - [8] Z. B. Stone and H. A. Stone, Imaging and quantifying mixing in a model droplet micromixer, *Phys. Fluids* **17**, 063103 (2005).
 - [9] T. Ward and G. Homsy, Chaotic streamlines in a translating drop with uniform electric field, *J. Fluid Mech.* **547**, 215 (2006).
 - [10] K. Bajer and H. K. Moffatt, On a class of steady confined Stokes flows with chaotic streamlines, *J. Fluid Mech.* **212**, 337 (1990).
 - [11] X. Xu and G. M. Homsy, Three-dimensional chaotic mixing inside drops driven by a transient electric field, *Phys. Fluids* **19**, 013102 (2007).
 - [12] M. D. Bryden and H. Brenner, Mass-transfer enhancement via chaotic laminar flow within a droplet, *J. Fluid Mech.* **379**, 319 (1999).
 - [13] D. Kroujiline and H. A. Stone, Chaotic streamlines in a steady bounded three-dimensional Stokes flow, *Physica D* **130**, 105 (1999).
 - [14] J. M. Ottino, Mixing, chaotic advection, and turbulence, *Annu. Rev. Fluid Mech.* **22**, 207 (1990).
 - [15] A. I. Neishtadt, Change of an adiabatic invariant at a separatrix, *Sov. J. Plasma Phys.* **12**, 567 (1986).
 - [16] J. R. Cary, D. F. Escande, and J. L. Tennyson, Adiabatic-invariant change due to separatrix crossing, *Phys. Rev. A* **34**, 4256 (1986).
 - [17] D. L. Vainshtein, A. A. Vasiliev, and A. I. Neishtadt, Changes in the adiabatic invariant and streamline chaos in confined incompressible Stokes flow, *Chaos* **6**, 67 (1996).
 - [18] G. I. Taylor, Studies in electrohydrodynamics I. The circulation produced in a drop by an electric field, *Proc. R. Soc. London, Ser. A* **291**, 159 (1966).
 - [19] J. R. Melcher and G. I. Taylor, Electrohydrodynamics: A review of the role of interfacial shear stresses, *Annu. Rev. Fluid Mech.* **1**, 111 (1969).
 - [20] L. S. Chang, T. E. Carleson, and J. C. Berg, Heat and mass transfer to a translating drop in an electric field, *Int. J. Heat Mass Transfer* **25**, 1023 (1982).
 - [21] D. L. Vainchtein, J. Widloski, and R. O. Grigoriev, Mixing properties of steady flow in thermocapillary driven droplets, *Phys. Fluids* **19**, 067102 (2007).
 - [22] A. Neishtadt, C. Simo, and A. Vasiliev, Geometric and statistical properties induced by separatrix crossings in volume-preserving systems, *Nonlinearity* **16**, 521 (2003).
 - [23] D. L. Vainchtein and A. Abudu, Resonance phenomena and long-term chaotic advection in volume-preserving systems, *Chaos* **22**, 013103 (2012).